Facile characterization of metallic impurities in detonation nanodiamonds through selective combustion using standard techniques

Killian Henry, Mélanie Emo, Sébastien Diliberto, Sebastien Hupont, Jean-Charles Arnault, Hugues Girard, Marc Dubois, B. Vigolo

Facile characterization of metallic impurities in detonation nanodiamonds through selective combustion using standard techniques

Killian Henry[1,2], Mélanie Emo[1], Sébastien Diliberto[1], Sébastien Hupont[1], Jean-Charles Arnault[3], Hugues A. Girard[3], Marc Dubois[2], Brigitte Vigolo[1,*]

1 Université de Lorraine, CNRS, Institut Jean Lamour, UMR 7198, allée André Guinier 54000 Nancy, France

2 Université Clermont Auvergne, CNRS, ICCF UMR 6296, 24 av. Blaise Pascal, F-63178 Aubière, France

3 Université Paris-Saclay, CEA, CNRS, NIMBE, 91191 Gif sur Yvette, France

* Corresponding author e-mail: Brigitte.Vigolo@univ-lorraine.fr

Keywords: nanodiamonds ; metallic impurities ; impurity traces ; standard techniques ; selective combustion

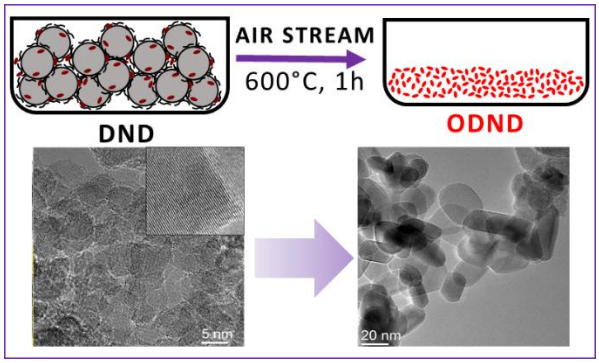

Graphical abstract

Abstract Detonation nanodiamonds are sp^3 carbon nanomaterials with narrow diameter distribution. They have high potential of application in various fields like nanomedecine,

advanced composites and lubricants, photocatalysis. Detonation nanodiamonds unfortunately contain metallic and inorganic impurities of diverse nature which can act as “Trojan horses” and even at weak content, they can significantly impact the nanodiamonds efficiency and the searched performances. Detection and quantification as well as subsequent removal of these impurities is highly difficult due to the lack of tools available by scholars. In this work, we propose a useful approach to detect and identify the inorganic impurities in detonation nanodiamonds. Our method which consists in a selective combustion of the nanodiamonds results in concentrating these impurities is a one-step and simple method. This approach, transferable to other kinds of carbon nanomaterials, is proved to be a valuable way allowing analysis of detonation nanodiamonds by standard characterization techniques such as X-ray Photoelectron Spectroscopy, Fourier Transform Infra-Red and Raman spectroscopies or Powder X-Ray Diffraction, available in any material science laboratory.

1 Introduction

After their confidential synthesis in the 1960s, detonation nanodiamonds (DNDs) have become fascinating nanomaterials over the world in the last thirty years. The detonation process is a powerful technique to produce NDs in high amount with a narrow distribution size and of rather high crystallinity [1]. Typically, DNDs are synthetized from mixtures of cyclotrimethylene trinitramine (RDX) and trinitrotoluene (TNT) leading to detonation reaction; high pressure and temperature allow then the formation of nanometric diamond crystallites. DNDs combine excellent thermal, mechanical and optical properties as well a high and chemically modifiable surface area [2–4]. DNDs are considered as ideal materials for applications over broad fields such as field emission, molecular sensing, heterogeneous catalysis… [5–9]. Their development for bioapplications such as cancer therapy, antimicrobial systems or drug delivery has increased in recent years. [10–18] Their use to

develop new slow neutron reflectors is another emerging research activity [19,20]; they have the potential to achieve a breakthrough in condensed matter since they could provide the unique technology to perfectly reflect slow neutrons. Pure DNDs could allow elastic or quasi-elastic scattering due to their low velocity and low thermal (cold) character making them particularly of great interest for study of condensed matter like colloids, biological molecules, polymers etc…

Unfortunately, DNDs contain a variety of inorganic impurities under the form of traces with a total content up to 2 - 3 wt.% [20–22]. Their origin is multiple: the reactor corrosion due to the harsh conditions during the detonation synthesis, the post-synthesis treatments for their separation from the other carbonaceous by-products and their post-synthesis purification [23,24]. These impurities, especially heavy metals, can have a negative impact on the DND properties to be exploited and they lead to non-desired and non-controlled effects: radioactivity through neutron interaction, toxicity by release into bodies, non-controlled optical phenomena…

The complete removal of these undesired metallic impurities within DNDs is currently not possible with efficacy [25–27]. Their detection by standard characterization techniques is impossible because of the weak content of each noncarbon impurity (below the Limit Of Detection, LOD). This difficulty renders it all the more difficult to develop efficient and simple purification approaches. It is as well important to note that each manufacturer or supplier has its own method of synthesis and post-purification, resulting in impurities of different natures and contents. There are multiple analytical methods suitable for direct identification of elemental impurities such as X-ray fluorescence (XRF), atomic absorption spectroscopy (AAS) or inductively coupled plasma-optical emission spectroscopy (ICP-OES),[24,28] but only a few techniques are sensitive enough to quantify ultra-traces of elements like in DNDs: inductively coupled plasma-mass spectrometry (ICP-MS) [22,23],

neutron (NAA) and prompt-gamma activation analyses (PGAA)[20,21]. Unfortunately, such equipment are seldom available in common material research laboratories especially for neutron activation based methods since they belong to large scientific instruments. It clearly appears there is a need of developing a simple approach allowing a facile detection and identification of the noncarbon byproducts in DNDs.

In this work, we propose to concentrate the inorganic part from DND samples by selectively burning off the DNDs. These residues can be then characterized by means of standard techniques whereas they fall below the LOD in the starting DNDs. Our approach, inspired from the core principle of elemental analysis techniques [22–24], proposes a simple method which allows to clearly identify the inorganic elements in DNDs and also the compounds (nature and crystalline phase) belonging to the DNDs. The proposed approach consists of thermally gasified the DND samples under air at 600°C, just above their combustion temperature. During the DND's combustion process, the metal-based impurities possibly undergone an oxidation reaction and their amount is finally substantially increased in the outcome ashes. Their analysis is consequently strongly facilitated. Furthermore, this treatment can be easily used by any scholars. We clearly show in this work that such method allows to overcome the long-term issue of detection and identification of the inorganic compounds in DNDs by standard characterization techniques: like X-ray diffraction (XRD), X-ray photoemission spectroscopy (XPS), Fourier Transform InfraRed (FTIR) and Raman spectroscopies. The proposed approach provides a universally accessible tool for the determination of the main DND's impurities and their relative quantification. The resulting better knowledge of DNDs is useful for developing efficient purification methods and can boost future applications of DNDs.

2 Experimental Section

2.1 Sample preparation

The used DNDs were provided by the Federal State Unitary Enterprise (FSUE) "Russian Federal Nuclear Center – Academician E.I. Zababakhin All-Russian Research Institute of Technical Physics" (RFNC-VNIIF institute, Snezhinsk, Russia). The production followed the Technical Regulation TY 2-037-677-94, were the DND were synthesized using a 60/40 mixture of TNT/RDX, and washed multiple times by acids. According to the RFNC-VNIIF institute, this procedure leads to nanoparticles with a mean diameter of 4-5 nm.

For the selective combustion of DND sample, approximately 1 g of the as-received powder was placed in a quartz boat then transferred into a quartz tube inside a tubular furnace. A pump was fixed to one extremity of the tube to provide an air flow of around 100 mL/min. The powder was therefore heated under air at 600 °C for one hour (10 °C/min), and then cooled under ambient conditions until reaching room temperature. The outcome sample was referred to as ODND. Since the content of the inorganic impurities (after oxidation) are around 1.8 wt.% (Figure 1f, insert), 1 g of starting DNDs gives rise to around 180 mg of residues which generates a sufficient quantity for several characterizations such as FTIR, Raman spectroscopy, XPS and Transmission Electronic Microscopy (TEM) since for each of them only less than 10 mg of sample are required.

2.2 Structural characterization

Powder XRD (PXRD) investigation was performed on a Bruker D8 advance diffractometer, in the Bragg-Brentano geometry with a Cu-source (λ_{Cu} = 1.54060 Å) equipped with a fast 1D LynkEye detector. Phase identification was performed using the Diffrac.Eva software V6.

The thermogravimetric analysis (TGA) was carried out using a Setaram Setsys evolution 1750 Thermal Gravimetric Analyzer. After loading the DND powder (around 10 mg) in an

alumina crucible, temperature was raised up to 900 °C under dry air at 5 °C/min with a flowrate of 20 mL/min. For the cooling, the rate was of 20 °C/min.

For TEM and High Resolution TEM (HRTEM) analysis, DNDs were dispersed in ethanol under sonication during 15 min. One droplet of the DND dispersion was deposited on a 200-mesh-size holey carbon grid provided by Delta Microscopies. The TEM observations were carried out using a JEOL JEM-ARM 200F Cold FEG apparatus equipped with a spherical aberration (Cs) probe corrector working at an accelerating voltage of 200 kV. For the sake of representativity of the sample, at least 50 images obtained at different locations on the sample were taken. In the TEM figures shown in the paper, representative images of DNDs are selected. Electron energy loss spectroscopy (EELS) and energy dispersive X-Ray spectroscopy (EDX) experiments were performed in scanning transmission electron microscopy (STEM) mode, as well as the high angle annular dark field (HAADF) images. X-maps and spectra were recorded on a Jeol spectrometer (SDD, Jeol DRY SD 30 GV). For EELS measurements, the spectrometer was set to an energy dispersion of 0.25 eV/channel to collect C-K, N-K, O-K, Cr-$L_{2,3}$ and Fe-$L_{2,3}$ edges.

FTIR spectrometry was performed using a Nicolet 6700 FT-IR (Thermo Scientific) spectrometer. Spectra were recorded in attenuated total reflectance (ATR; diamond crystal) mode using 100 scans and a resolution of 2 cm^{-1}.

The microRaman spectroscopy study was performed with a LabRAM HR 800 micro-Raman spectrometer. For the phase study for the ODND sample, a Torus diode laser with a wavelength of 532 nm provided by Laser Quantum was used. The energy received by the sample is around 4 mW/cm^2 at full power.

XPS spectra were collected on a Kratos Axis Ultra (Kratos Analytical, UK) spectrometer equipped with a monochromatic Al Kα (1486.6 eV). All spectra were recorded at a 90° takeoff angle. The high-resolution regions were acquired with 0.1 eV step and 20 eV pass

energy (instrumental resolution better than 0.5 eV). For the analysis, the powders were fixed onto a copper scotch tape. Curve fitting was performed using a combined Gaussian and Lorentzian line profile after Shirley's background subtraction by Casa XPS software.

Regarding ICP-MS the quadrupole ICP-MS is an iCAPQ (ThermoElectron) classically equipped with a cyclonic glass nebulization chamber (tuned in high matrix mode, with a dwell time set to 40 ms) and a nanoparticle glass nebulizer (Glass Expansion). A collision cell is used to avoid molecular ions that could be formed in the argon plasma. Samples are analyzed by external calibration in the range 5 to 150 ppb. All dilutions are performed by weight. Barium, copper, aluminum, iron, zinc, calcium, sodium and lead standards solution are obtained by dilution from a SPEX CertiPrep Claritas and 2 % hydrochloric acid purified by sub-boiling distillation. Samples are constantly placed inside an ultrasonic bath.

3 Results and Discussion

3.1 Concentration of inorganic impurities by selective combustion of DNDs

TEM observations show DNDs aggregates or chaplets of several hundreds of nm in size (Figures 1a-1b), as typically observed for the NDs synthesized by the detonation method [29–32]. An example of HRTEM image is depicted in Figure 1c. The insert exhibits lattice planes of the DNDs, showing the crystallized structure of the material [29,33,34]. The size distribution, over a total of 183 nanoparticles measured, follows a log normal distribution behavior centered around 5.6 ± 1.8 nm, which is in agreement with the mean diameter of 4-5 nm given by the supplier (Figure 1d).

PXRD pattern of the studied DNDs exhibits the five reflections expected for the diamond phase in the ICCD database (PDF#06-0675): (111) at 42°, (222) at 75°, (311) at 90°, (400) at 120° and (331) at 140°. By applying the Scherrer law on the (111) peak, a value of 4.2 nm

was found for the crystallite size, which is in accordance with the TEM analysis. The experimental diffractogram of DNDs (black) matches quite well with the XRD pattern simulated with CaRine software (red). The broad peak observed from 20-40° seems to belong to the (002) reflection of a sp^2 layers surrounding the DND particles [35–37], as suggested on upper left particle in Figure 1c.

Figure 1f exhibits the thermogram performed under air of the raw DNDs. After dehydration of the DNDs at around 120 °C, the major weight loss around 500°C corresponds to the DND complete combustion. Above 600 °C, the total amount of the inorganic impurities present in DNDs is around ~ 1.8 wt.% (inset Figure 1f). Those which are not already of an oxidized form have undergone an oxidation during TGA under air, which is confirmed by the weight gain observed in the 300-425 °C range.

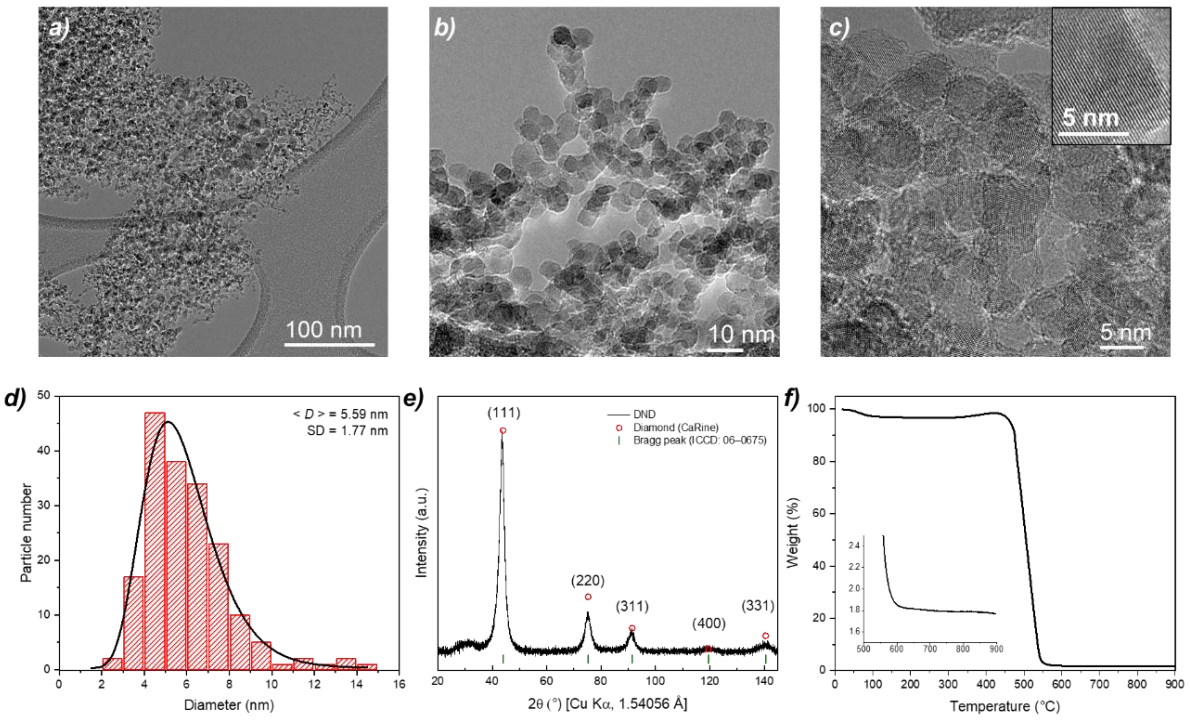

Figure 1 a)-b) TEM images of detonation nanodiamonds at different magnifications and c) HRTEM image of the same sample, insert: zoom-in on a ND particle. d) Size distribution of DND with a log normal distribution function (black curve), calculated based on 183 particles. The mean diameter is note < *D* >, while the standard deviation is abbreviated SD. e) PXRD

pattern (Cu, 1.5406 Å) of as-received DND. The black line is the experimental pattern, the red circles are the simulated pattern for diamond, based on CaRine software, green bars indicate the position of (hkl) planes from the ICCD #06-0675 file. f) Thermogram of DND under dry air. The insert is a zoom in the high temperature range showing the remaining mass after the complete consumption of the DNDs.

Figure 2 illustrates the developed selective combustion of detonation nanodiamond method. Temperature is raised up to above the DND burnt off (*i.e.* 600°C) determined from TGA (Figure 1f) and the remaining inorganic impurities are thus naturally concentrated.

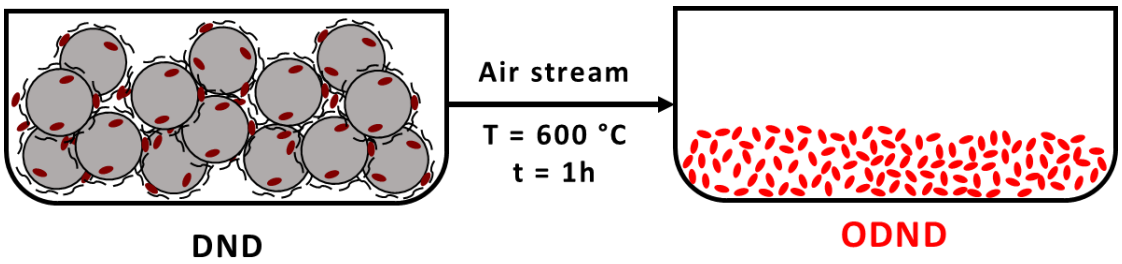

Figure 2 Selective combustion of the detonation nanodiamonds leading to the outcome ODND sample. DNDs are represented as grey solid circles surrounded by some graphite layers (in black) and inorganic impurities (in brown). The resulting ashes (ODND) are displayed in red.

3.2 Determination of the main impurities in DND and ODND

The inorganic impurities (total amount of ~ 1.8 wt.%) present in the raw DND powder have many origins and they are of numerous natures. Their detection is consequently a tricky task since their respective content is below the LOD of most of the standard characterization techniques. Thanks to local techniques such as EDX and EELS analysis, some impurities, certainly those being present at the highest concentration in DNDs, could be detected.

Although local, such scrutinized investigation is required before quantitative analysis by using ICP-MS which is indeed not possible in a blind manner.

3.2.1 The main inorganic impurities in DNDs

The TEM observation of inorganic impurities in DND was made possible by the use of high angle annular dark field (HAADF) images in scanning mode. Thus, EDX spectroscopy analyses were performed to determine the elemental composition of these particles. Also, X-maps were acquired to localize precisely the inorganic elements. In Figure 3a, two brighter spots are visible in the HAADF STEM, one is constituted of carbon (Figure 3b), while the upper left particle is composed of two metallic elements: iron and chromium (Figures 3e-3f). Also, oxygen is localized in the upper left particle, presuming a Cr/Fe-oxide based particle (Figures 3d-3f). The size of the observed particles in DND is typically of 30-40 nm. A complementary EELS experiment was carried out in another region and signals of O K-edge, Cr and Fe L-edges were recorded, together with C and N K-edges (Figure S1, Supporting Information). By investigated other areas of the DND sample, different particles were found with distinct compositions (Figure S2, Supporting Information): one is composed of O, S and Ba, while the other is constituted of O, Si, K, Cr and Fe. The fact that chromium and iron were found in multiple particles seems to further confirm their distribution in the whole sample as the main impurities. Also, a large particle constituted of Si and O was observed (Figure S3, Supporting Information), probably originating from fragments of laboratory glassware used for the purification of DND.

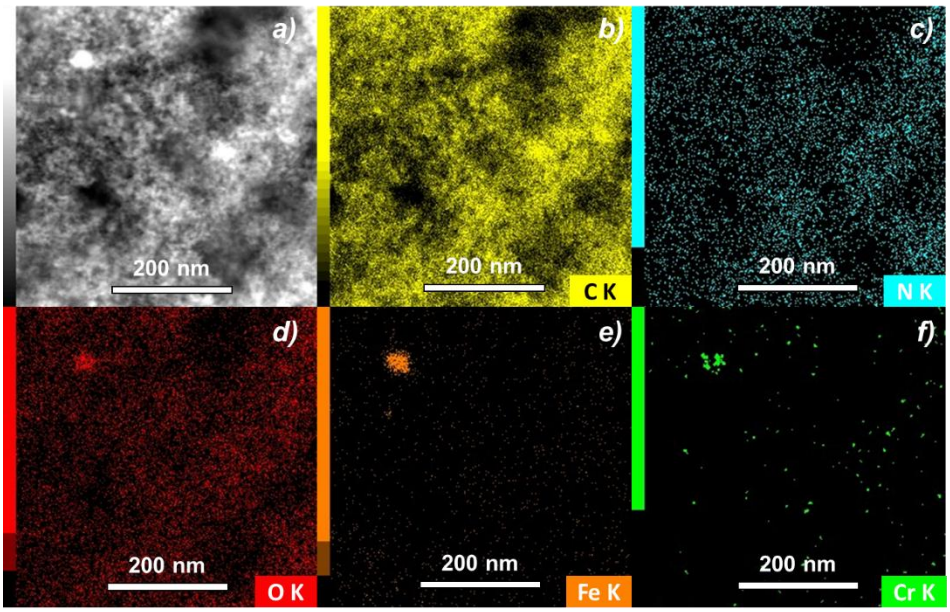

Figure 3 a) High angle annular dark field (HAADF) STEM image of a selected area of the as-received DND, and b-f) corresponding EDX spectroscopy elemental mappings. Carbon signal is shown in yellow (b), nitrogen in light blue (c) and oxygen in red (d). Iron (e) and cobalt (f) are respectively represented by orange and green colors.

3.2.2 Determination of elements as impurities in ODND by local and bulk analysis

By TEM, the outcome residues appear as several spherical and elongated particles (Figures 4a-4c and Figures S5-S6, Supporting Information) of a size typically in the 20-40 nm range (Figure S4, Supporting Information) in agreement with the non-carbon particle size observed in DND sample (Figure 3). From the TEM observations made on several zones of the ODND sample and the analysis of 50 micrographs, no nanodiamond was noticed. By EDX spectroscopy elemental mapping, silicon, chromium and iron could be detected in agreement with DND analysis. Cr and Fe are most often localized within the same particles (Figure 4 and Figure S5, Supporting Information) and in some areas, chromium oxides are found without presence of iron (Figure S6, Supporting Information). Aluminum and titanium were as well detected (Figures S5 and S6, Supporting Information).

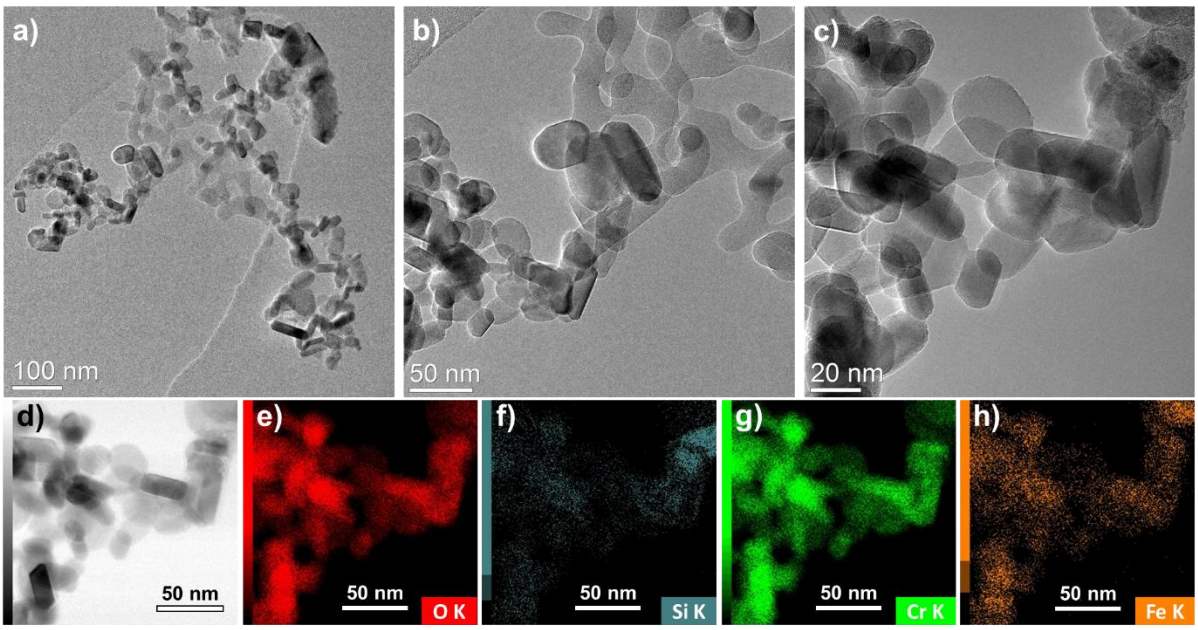

Figure 4 a-c) TEM images of ODND at different magnifications. d) corresponding bright-field STEM image of c). e-h) EDX spectroscopy elemental mapping of O-, Si-, Cr- and Fe K-edges, respectively.

To confirm the presence of the above listed elements, a XPS analysis of DND and ODND powders was performed, and shown in Figure 5. In DNDs (Figure 5a), only C, N, O and S could be observed, while for ODND (Figure 5b) a few metallic elements were seen: Na, Al, Si, Cr and Fe. The observed elements are in good agreement with EDX study above (Figure 4, Figures S4 and S5, Supporting Information). The fact that no traces of Ti was detected in the XPS spectrum of ODND could signify its content is very weak. For Na, since the TEM analysis is a local technique, observations were certainly done in the areas where it is not present.

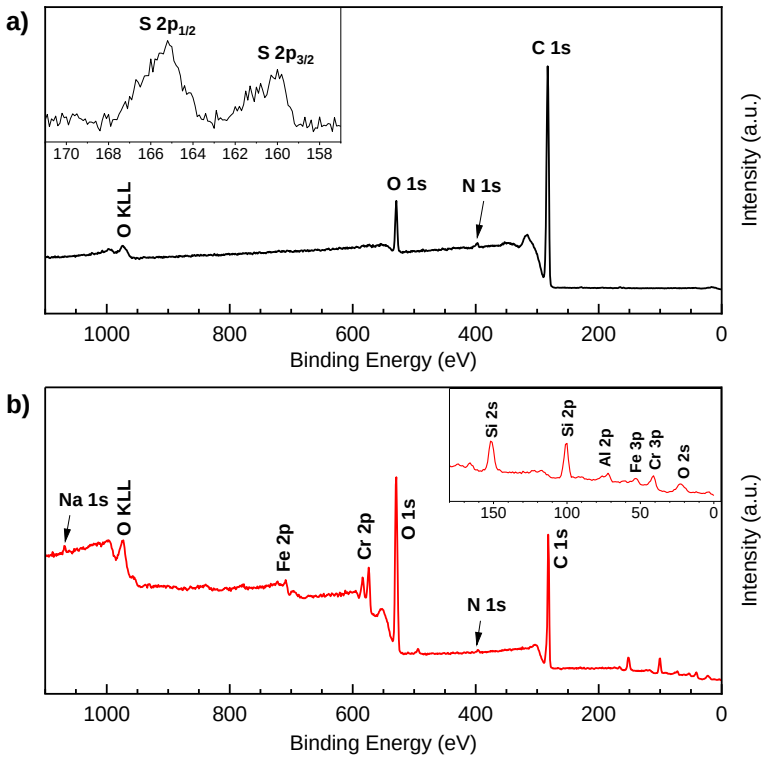

Figure 5 XPS survey scans of a) DND and b) ODND.

To summarize from local (EDX spectroscopy) and bulk techniques (XPS), Si, Cr and Fe may be considered as the main metallic elements in DND. Na, Al and Ti seem to be present in weaker amount.

3.2.3 Reliability of the selective combustion of nanodiamonds approach

Analysis from ICP-MS, shown below in Figure 6, provides the contents of the main heteroelements present in both DND and ODND samples. In agreement with EDX spectroscopy analysis, ICP-MS shows that Si, Cr and Fe are the main impurities in the DND sample. Cu, Al, Na, Pb, Ba, Ti and Ca are at least 5 times less concentrated than the three main elements. Zn is present as traces in DND (2.10^{-3} wt.%).

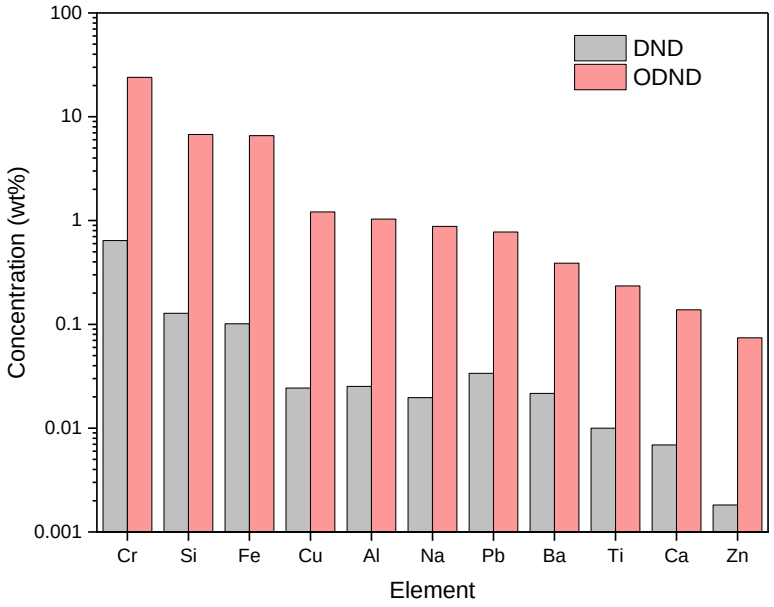

Figure 6 ICP-MS elemental analysis of DND (grey) and ODND (red). The detected elements are as function of their concentration in weight percent. For visibility purposes, a log-scale was used.

Table 1 gives the content of the main elements in DND and ODND. The corresponding ratios of each element with respect with Cr, the main impurity found, fall in the same range for both samples, proving that ODND provides a reliable insight of the metallic impurities of DND. These latter concentrated in the thermally treated DNDs make possible their further detection and analysis by standard techniques, as shown in the following.

The impurities in DND samples supplied by the RFNC-VNIIF institute were investigated by other techniques, such as NAA [20], and AES [38], with the need of ICP-MS [23], and are in good agreement with Table 1.

Table 1 Content of the elements found in DND and ODND from ICP-MS and their relative content with respect with Cr, the most concentrated heteroatom impurity.

Element	DND		ODND	
	wt.%	Factor of dilution with respect to Cr	wt.%	Factor of dilution with respect to Cr
Cr	0.641	--	23.965	--
Si	0.128	6	6.745	3.5
Fe	0.101	6	6.582	3.6
Cu	0.024	30	1.212	20
Al	0.025	20	1.033	24
Na	0.020	30	0.880	27
Pb	0.034	20	0.776	30
Ba	0.022	60	0.388	60
Ti	<0.01	60	0.235	120
Ca	0.007	60	0.138	240
Zn	0.002	300	0.074	240

3.3 DND impurity detection and determination of their nature and origin

Identification of the compounds in DND after being treated under air and determination of the corresponding impurity nature in DND were first based on PXRD investigation. A typical diffractogram of ODND is displayed in Figure 7 where numerous peaks are observable. For their assignment, the elements already known to be present from XPS and EDX analyses and the reported chemical treatments undergone by the used as-produced DNDs have been considered. In the following, the main compounds determined in ODND are described one by one along with the results from different characterization methods complementary to PXRD in order to ascertain their presence.

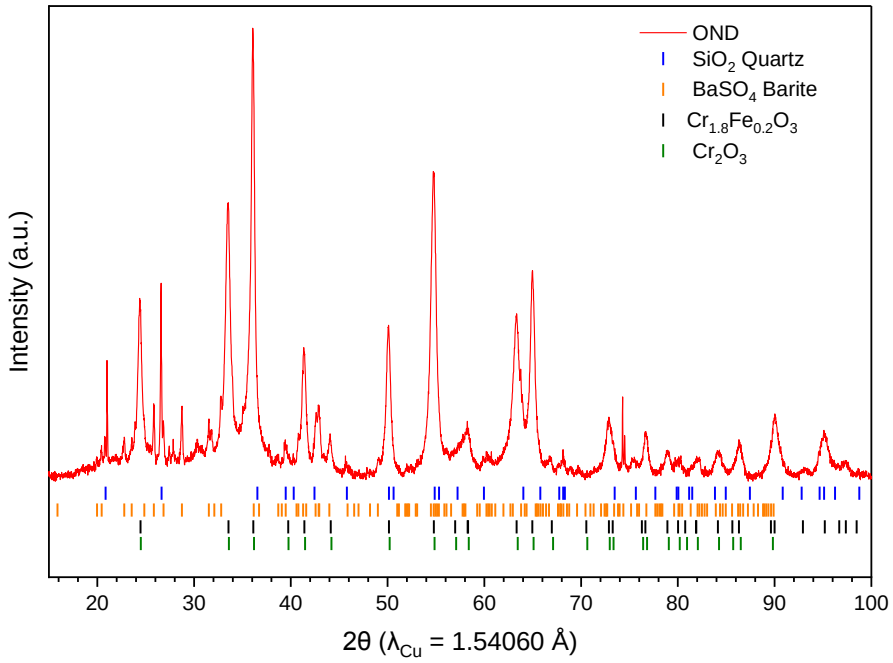

Figure 7 PXRD pattern of ODND, performed with a Cu source (λ_{Cu} = 1.5406 Å). Five possible phases were indexed, and shown as colored stick: quartz SiO_2 (PDF 46-1045) in blue, barite $BaSO_4$ (PDF 83-2053) in orange, $Cr_{1.8}Fe_{0.2}O_3$ (PDF 04-006-8202) in black and chromium oxide Cr_2O_3 (PDF 85-0730) in green.

3.3.1 Silicon – SiO_2

Silicon is one of the main elements detected in both DND and ODND by EDX spectroscopy and XPS. From EDX mapping, silicon was most often observed in the same area than that of oxygen, which seems to make clear that silicon oxide (SiO_2) is present in both samples (Figure 4, Figures S3, S5 and S6, Supporting Information). The α-quartz phase could be identified in ODND by PXRD (Figure 7), and further confirmed by Raman (Figure S7, Supporting Information) and FTIR spectroscopies (Figure S8, Supporting Information), where all Raman- and IR-actives bands of SiO_2 were observed.

3.3.2 Chromium and iron – Cr_2O_3, Fe_2O_3 and $Cr_{2-x}Fe_xO_3$

Figure S6 clearly indicates there are areas were chromium oxides are not surrounded by iron, being the sign of presence of pure chromium oxides, possibly Cr_2O_3, since it is the most stable oxide form of chromium at 600°C [39]. Also, chromium oxides are commonly found in literature as residual impurities of DNDs. $BaCrO_4$ is used as detonator/initiator for DND synthesis and a mixture of H_2SO_4 and CrO_3 or $K_2Cr_2O_7$ (Jones oxidation) have been reported to be used as oxidant for post-synthesis purification by the supplier [23]. Thus, all chromium residuals could have been altered during the combustion of the DND, leading to chromium oxides.

Raman spectroscopy on DNDs thermally treated under air (Figures S9 and S10) have revealed the presence of Cr_2O_3, which is in agreement with the TEM observation (Figure S6, Supporting Information), but also the presence of the solid solution $Cr_{2-x}Fe_xO_3$ characterized in the spectrum by the addition of three magnon peaks. This could explain the systematic presence of Fe alongside Cr and O during our TEM observation in the last section. This is not surprising since the detonation chamber is composed of steel alloys that might contain Cr, as well as other metals.

On the other side, FTIR spectroscopy (Figure S8) shows all the typical vibration modes of Cr_2O_3. Also, since the spectrum is composed of multiple overlapping contributions, some peaks might correspond to the vibration modes of Fe_2O_3. However, it is not possible to confirm if they belong to pristine material (α- or γ-Fe_2O_3), the most probable origin of these peaks is due to the presence of iron in the $Cr_{2-x}Fe_xO_3$ solid-solution.

Therefore, the diffractogram of ODND in Figure 7 can be indexed by both Cr_2O_3 and $Cr_{2-x}Fe_xO_3$. However, it is impossible to know the exact level of iron substitution inside the compound, thus the $Cr_{1.8}Fe_{0.2}O_3$ phase was chosen since it matches perfectly with the diffraction peaks observed.

3.3.3 Barium – Barite $BaSO_4$

Barite ($BaSO_4$), *Pnma* (62), can be well identified by PXRD (Figure 7). It has already been reported as residual impurity after acidic-purification treatment [23,25]. As mentioned early, $BaCrO_4$ being a detonator/initiator during the detonation process certainly remains in DND. Its reaction with sulfuric acid by the post-synthesis purification treatment could explain the detection of $BaSO_4$ by PXRD [23,25].

3.4 Investigation of DNDs by standard and non-standard techniques

Table 2 summarizes the results found from the conducted in-depth analysis of DND and ODND by means of standard and non-standard methods as defined below. Characterization of the thermally DND treated under air by non-standard techniques leads to similar results than those found for as-produced DND and its characterization by standard techniques allows to determine the heteroatoms present in DND in a simple manner.

Table 2 Classification of the material characterization techniques depending on their specificity of use and on their ability to detect and identify the impurities in DND and ODND.

	Technique	Elements/Phase detected	
		DND	**ODND**
Non-standard characterization techniques*	Inductively Coupled Plasma Mass Spectrometry (ICP-MS)	Cr, Si, Fe, Cu, Al, Na, Pb, Ba, Ca, Ti, Zn	Cr, Si, Fe, Cu, Al, Na, Pb, Ba, Ca, Ti, Zn
	Transmission Electron microscopy (TEM) / EDX-mapping	C, N, O, S, Si, Cr, Fe, Ba	C, N, O, Al, Si, Ti, Cr, Fe, Ba
Standard characterization techniques**	X-ray diffraction (XRD)	$C_{diamond}$	SiO_2, $BaSO_4$, Cr_2O_3, $Fe_xCr_{2-x}O_3$
	Fourier Transform Infrared spectroscopy (FTIR) – ATR mode	$C_{diamond}$	SiO_2, Cr_2O_3
	Raman spectroscopy	$C_{diamond}$	SiO_2, Cr_2O_3, $Fe_xCr_{2-x}O_3$
	X-ray photoelectron spectrometry (XPS)	C, N, O, S	C, N, O, Cr, Fe, Al, Si, Na

*A characterization technique is considered as non-standard if its accessibility is restrained because of, for example, proposal submission process for very large instruments or a specific sample preparation required or very long exposure time and a high which-how is required to run the experiments so that the material science scholars cannot run the analysis themselves.

** A standard characterization technique requires an available equipment in common material laboratories. Such technique is easy to use without with simple sample preparation and fast result delivery with reasonable data treatment and fitting.

4 Conclusion

In this work, we have developed an alternative approach which provides a useful tool to overcome the long-standing issues of hidden metallic impurities in DNDs. The noncarbon impurities could be concentrated by simply applied a combustion treatment to DND in air. Both as-received and thermally treated under air DND samples were analyzed by means of commonly available local and bulk characterization methods. The developed approach has been proven to be reliable and allows to follow in a simple manner the inorganic element content and their nature in DND samples. This process can be applied after any chemical treatment or modifications of DND. The proposed approach could hence help scholars in developing further applications of DNDs and it could become a universal process to concentrate the metallic impurities contained of any kind of carbonaceous nanomaterial to overcome the limit of detection of standard characterization techniques.

Acknowledgments

B.V. and K.H. would like to thank Lionel Aranda for his valuable help in TGA experiments. The authors are grateful to ANR for the funding of this work with the project NERF (ANR-20-CE08-0034).

References

[1] V.Y. Dolmatov, A.N. Ozerin, I.I. Kulakova, O.O. Bochechka, N.M. Lapchuk, V. Myllymäki, A. Vehanen, Detonation nanodiamonds: new aspects in the theory and practice of synthesis, properties and applications, Russ. Chem. Rev. 89 (2020) 1428. https://doi.org/10.1070/RCR4924.

[2] I.I. Kulakova, Surface chemistry of nanodiamonds, Phys. Solid State. 46 (2004) 636–643. https://doi.org/10.1134/1.1711440.

[3] V.N. Mochalin, O. Shenderova, D. Ho, Y. Gogotsi, The properties and applications of nanodiamonds, Nature Nanotech. 7 (2012) 11–23. https://doi.org/10.1038/nnano.2011.209.

[4] G. Reina, L. Zhao, A. Bianco, N. Komatsu, Chemical Functionalization of Nanodiamonds: Opportunities and Challenges Ahead, Angewandte Chemie International Edition. 58 (2019) 17918–17929. https://doi.org/10.1002/anie.201905997.
[5] M.L. Terranova, S. Orlanducci, M. Rossi, E. Tamburri, Nanodiamonds for field emission: state of the art, Nanoscale. 7 (2015) 5094–5114. https://doi.org/10.1039/C4NR07171A.
[6] E. Janitz, K. Herb, L.A. Völker, W.S. Huxter, C.L. Degen, J.M. Abendroth, Diamond surface engineering for molecular sensing with nitrogen—vacancy centers, J. Mater. Chem. C. 10 (2022) 13533–13569. https://doi.org/10.1039/D2TC01258H.
[7] A.V. Shvidchenko, E.D. Eidelman, A.Ya. Vul', N.M. Kuznetsov, D.Yu. Stolyarova, S.I. Belousov, S.N. Chvalun, Colloids of detonation nanodiamond particles for advanced applications, Advances in Colloid and Interface Science. 268 (2019) 64–81. https://doi.org/10.1016/j.cis.2019.03.008.
[8] N. Nunn, M. Torelli, G. McGuire, O. Shenderova, Nanodiamond: A high impact nanomaterial, Current Opinion in Solid State and Materials Science. 21 (2017) 1–9. https://doi.org/10.1016/j.cossms.2016.06.008.
[9] S. Navalón, A. Dhakshinamoorthy, M. Álvaro, H. García, Diamond Nanoparticles in Heterogeneous Catalysis, Chem. Mater. 32 (2020) 4116–4143. https://doi.org/10.1021/acs.chemmater.0c00204.
[10] A.S. Barnard, Predicting the impact of structural diversity on the performance of nanodiamond drug carriers, Nanoscale. 10 (2018) 8893–8910. https://doi.org/10.1039/C8NR01688G.
[11] N. Bondon, L. Raehm, C. Charnay, R. Boukherroub, J.-O. Durand, Nanodiamonds for bioapplications, recent developments, J. Mater. Chem. B. 8 (2020) 10878–10896. https://doi.org/10.1039/D0TB02221G.
[12] M. Bilal, H. Cheng, R.B. González-González, R. Parra-Saldívar, H.M.N. Iqbal, Bio-applications and biotechnological applications of nanodiamonds, Journal of Materials Research and Technology. 15 (2021) 6175–6189. https://doi.org/10.1016/j.jmrt.2021.11.037.
[13] S. Chauhan, N. Jain, U. Nagaich, Nanodiamonds with powerful ability for drug delivery and biomedical applications: Recent updates on in vivo study and patents, Journal of Pharmaceutical Analysis. 10 (2020) 1–12. https://doi.org/10.1016/j.jpha.2019.09.003.
[14] N. Prabhakar, J.M. Rosenholm, Nanodiamonds for advanced optical bioimaging and beyond, Current Opinion in Colloid & Interface Science. 39 (2019) 220–231. https://doi.org/10.1016/j.cocis.2019.02.014.
[15] R. Namdar, S. Nafisi, Nanodiamond applications in skin preparations, Drug Discovery Today. 23 (2018) 1152–1158. https://doi.org/10.1016/j.drudis.2018.04.006.
[16] M. Barzegar Amiri Olia, P.S. Donnelly, L.C.L. Hollenberg, P. Mulvaney, D.A. Simpson, Advances in the Surface Functionalization of Nanodiamonds for Biological Applications: A Review, ACS Appl. Nano Mater. 4 (2021) 9985–10005. https://doi.org/10.1021/acsanm.1c02698.
[17] A.M. Schrand, S.A.C. Hens, O.A. Shenderova, Nanodiamond Particles: Properties and Perspectives for Bioapplications, Critical Reviews in Solid State and Materials Sciences. 34 (2009) 18–74. https://doi.org/10.1080/10408430902831987.
[18] J.-X. Qin, X.-G. Yang, C.-F. Lv, Y.-Z. Li, K.-K. Liu, J.-H. Zang, X. Yang, L. Dong, C.-X. Shan, Nanodiamonds: Synthesis, properties, and applications in nanomedicine, Materials & Design. 210 (2021) 110091. https://doi.org/10.1016/j.matdes.2021.110091.
[19] V. Nesvizhevsky, R. Cubitt, E. Lychagin, A. Muzychka, G. Nekhaev, G. Pignol, K. Protasov, A. Strelkov, Application of Diamond Nanoparticles in Low-Energy Neutron Physics, Materials. 3 (2010) 1768–1781. https://doi.org/10.3390/ma3031768.
[20] V. Nesvizhevsky, U. Köster, M. Dubois, N. Batisse, L. Frezet, A. Bosak, L. Gines, O. Williams, Fluorinated nanodiamonds as unique neutron reflector, Carbon. 130 (2018) 799–805. https://doi.org/10.1016/j.carbon.2018.01.086.
[21] R.Yu. Yakovlev, N.N. Dogadkin, I.I. Kulakova, G.V. Lisichkin, N.B. Leonidov, V.P. Kolotov, Determination of impurities in detonation nanodiamonds by gamma activation analysis

method, Diamond and Related Materials. 55 (2015) 77–86. https://doi.org/10.1016/j.diamond.2015.03.010.
[22] D.P. Mitev, A.T. Townsend, B. Paull, P.N. Nesterenko, Direct sector field ICP-MS determination of metal impurities in detonation nanodiamond, Carbon. 60 (2013) 326–334. https://doi.org/10.1016/j.carbon.2013.04.045.
[23] D.P. Mitev, A.T. Townsend, B. Paull, P.N. Nesterenko, Screening of elemental impurities in commercial detonation nanodiamond using sector field inductively coupled plasma-mass spectrometry, J Mater Sci. 49 (2014) 3573–3591. https://doi.org/10.1007/s10853-014-8036-3.
[24] P.N. Nesterenko, D. Mitev, B. Paull, Chapter 5 - Elemental analysis of nanodiamonds by inductively coupled plasma hyphenated methods, in: J.-C. Arnault (Ed.), Nanodiamonds, Elsevier, 2017: pp. 109–130. https://doi.org/10.1016/B978-0-32-343029-6.00005-2.
[25] D.P. Mitev, A.T. Townsend, B. Paull, P.N. Nesterenko, Microwave-assisted purification of detonation nanodiamond, Diamond and Related Materials. 48 (2014) 37–46. https://doi.org/10.1016/j.diamond.2014.06.007.
[26] V.Yu. Dolmatov, A. Vehanen, V. Myllymäki, K.A. Rudometkin, A.N. Panova, K.M. Korolev, T.A. Shpadkovskaya, Deep purification of detonation nanodiamond material, J. Superhard Mater. 35 (2013) 408–414. https://doi.org/10.3103/S1063457613060099.
[27] S.P. Hong, T.H. Kim, S.W. Lee, Plasma-assisted purification of nanodiamonds and their application for direct writing of a high purity nanodiamond pattern, Carbon. 116 (2017) 640–647. https://doi.org/10.1016/j.carbon.2017.02.040.
[28] Trace and Ultratrace Elemental Analysis, in: ACS Reagent Chemicals, American Chemical Society, Washington, DC, 2017. https://doi.org/10.1021/acsreagents.2006.20200501.
[29] V.N. Mochalin, O. Shenderova, D. Ho, Y. Gogotsi, The properties and applications of nanodiamonds, Nature Nanotech. 7 (2012) 11–23. https://doi.org/10.1038/nnano.2011.209.
[30] V.Yu. Dolmatov, T. Fujimura, Physical and Chemical Problems of Modification of Detonation Nanodiamond Surface Properties, in: D.M. Gruen, O.A. Shenderova, A.Ya. Vul' (Eds.), Synthesis, Properties and Applications of Ultrananocrystalline Diamond, Springer Netherlands, Dordrecht, 2005: pp. 217–230. https://doi.org/10.1007/1-4020-3322-2_16.
[31] V. Danilenko, O.A. Shenderova, Chapter 5 - Advances in Synthesis of Nanodiamond Particles, in: O.A. Shenderova, D.M. Gruen (Eds.), Ultananocrystalline Diamond (Second Edition), William Andrew Publishing, Oxford, 2012: pp. 133–164. https://doi.org/10.1016/B978-1-4377-3465-2.00005-0.
[32] P.M.V. Baidakova, Methods of Characterization and Models of Nanodiamond Particles, in: Detonation Nanodiamonds, Jenny Stanford Publishing, 2013.
[33] A. Krueger, The structure and reactivity of nanoscale diamond, J. Mater. Chem. 18 (2008) 1485. https://doi.org/10.1039/b716673g.
[34] M. Baidakova, A. Vul', New prospects and frontiers of nanodiamond clusters, J. Phys. D: Appl. Phys. 40 (2007) 6300–6311. https://doi.org/10.1088/0022-3727/40/20/S14.
[35] J. Chen, S.Z. Deng, J. Chen, Z.X. Yu, N.S. Xu, Graphitization of nanodiamond powder annealed in argon ambient, Appl. Phys. Lett. 74 (1999) 3651–3653. https://doi.org/10.1063/1.123211.
[36] A.P. Puzyr, V.S. Bondar, A.A. Bukayemsky, G.E. Selyutin, V.F. Kargin, Physical and Chemical Properties of Modified Nanodiamonds, in: D.M. Gruen, O.A. Shenderova, A.Ya. Vul' (Eds.), Synthesis, Properties and Applications of Ultrananocrystalline Diamond, Springer Netherlands, Dordrecht, 2005: pp. 261–270. https://doi.org/10.1007/1-4020-3322-2_20.
[37] V.Yu. Osipov, F.M. Shakhov, K.V. Bogdanov, K. Takai, T. Hayashi, F. Treussart, A. Baldycheva, B.T. Hogan, C. Jentgens, High-Quality Green-Emitting Nanodiamonds Fabricated by HPHT Sintering of Polycrystalline Shockwave Diamonds, Nanoscale Res Lett. 15 (2020) 209. https://doi.org/10.1186/s11671-020-03433-7.
[38] V.Yu. Dolmatov, 11 - Synthesis and Post-Synthesis Treatment of Detonation Nanodiamonds, in: O.A. Shenderova, D.M. Gruen (Eds.), Ultrananocrystalline Diamond, William Andrew

Publishing, Norwich, NY, 2006: pp. 347–377. https://doi.org/10.1016/B978-081551524-1.50013-5.
[39] B.L. Chamberland, The chemical and physical properties of CrO_2 and tetravalent chromium oxide derivatives, Critical Reviews in Solid State and Materials Sciences. 7 (1977) 1–31. https://doi.org/10.1080/10408437708243431.